Mineralogical Magazine, June 2000, Vol. 64(3), pp. 569–576

Letters

Crystal structure of the high-pressure monoclinic phase-II of cristobalite, SiO_2

M. T. DOVE[1,*], M. S. CRAIG[1], D. A. KEEN[2], W. G. MARSHALL[2], S. A. T. REDFERN[1], K. O. TRACHENKO[1] AND M. G. TUCKER[1]

[1] Department of Earth Sciences, University of Cambridge, Downing Street, Cambridge CB2 3EQ, UK
[2] ISIS Facility, Rutherford Appleton Laboratory, CLRC, Chilton, Didcot, Oxfordshire OX11 0QX, UK

ABSTRACT

The crystal structure of the high-pressure phase-II of cristobalite has been solved by neutron diffraction (space group $P2_1/c$, a = 8.3780(11) Å, b = 4.6018(6) Å, c = 9.0568(13) Å, β = 124.949(7)°, at P = 3.5 GPa). This phase corresponds to a distortion of the high-temperature cubic β-phase, rather than of the ambient temperature and pressure tetragonal α-phase.

KEYWORDS: cristobalite, high-pressure, neutron diffraction, phase transitions.

Introduction

SILICA, SiO_2, is a model system among materials that are important in geology, technology and other physical and chemical sciences. It has a rich phase diagram, containing both stable and metastable phases. Because of its importance, it is very useful to be able to characterize and understand the origin of new phases. Several groups have noted that the cristobalite polymorph of silica transforms to a new phase on increasing pressure. The most careful work was carried out by Palmer and Finger (1994) using diffraction by synchrotron radiation at ambient temperature. They showed that a high-pressure phase exists for pressures above *ca* 1.5 GPa (there is some variation in this value), with a primitive monoclinic structure. Palmer and Finger (1994) were able to index their diffraction patterns, and from their unit cell parameters they were able to deduce the strains that accompany the phase transition. No crystal structure data were reported, however. More recently Onodera *et al.* (1997) have extended these data to higher temperatures, showing that the slope of the α–II P–T phase boundary is negative.

Given the similarities of the unit cell dimensions of the new high-pressure monoclinic phase-II and the ambient-pressure tetragonal α-phase (space group $P4_12_12$; Palmer and Finger, 1994), and the similarities of the Raman spectra from the two phases (Palmer *et al.*, 1994), it is probable that the two phases are related as through a displacive phase transition. This immediately leads to the idea that the monoclinic phase-II is obtained as a displacive instability of the tetragonal α-phase, and based on this argument Palmer and Finger (1994) suggested that the monoclinic phase-II should have space group $P2_1$. Moreover, these authors were also able to identify the wave vector in the Brillouin zone of space group $P4_12_12$ that would correspond to a soft mode for such a phase transition, based on the tables of Stokes and Hatch (1988). However, Hammonds *et al.* (1996) pointed out possible difficulties with this scenario. In particular, application of their 'Rigid Unit Mode' model showed that any soft mode for this wave vector in the tetragonal phase would need to be accompanied by significant distortions of the SiO_4 tetrahedra, and it had previously been found that most phase transitions in framework silicates occurred through soft modes in which the tetrahedra are not distorted, at least to first order. Our own (unpublished) calculations of the phonon spectrum of the tetragonal α-phase of cristobalite over a wide range of pressures using the interatomic potential of Sanders *et al* (1984) and the GULP program of Gale (1997) indicate that there are no soft modes in the tetragonal phase on increasing pressure.

* E-mail: martin@esc.cam.ac.uk

Hammonds *et al.* (1996) suggested an alternative mechanism for the phase transition to the monoclinic phase-II. The important point they made is that the structure of phase-II could arise by a displacive distortion of the high-temperature cubic β-phase of cristobalite instead of by a displacive distortion of the low-temperature α-phase. Moreover, the tables of Stokes and Hatch (1988) show that a monoclinic phase of space group $P2_1/c$ with appropriate unit cell dimensions can arise as a distortion of the cubic phase involving a soft-mode with wave vector **L** = (½,½,½). In this model the relationship between the unit cells of the monoclinic and cubic unit cell vectors can be represented by the transformation matrix equation,

$$\begin{pmatrix} \mathbf{a} \\ \mathbf{b} \\ \mathbf{c} \end{pmatrix}_{P2_1/c} = \begin{pmatrix} -\frac{1}{2} & -\frac{1}{2} & 1 \\ \frac{1}{2} & -\frac{1}{2} & 0 \\ 1 & 1 & 0 \end{pmatrix} \times \begin{pmatrix} \mathbf{a} \\ \mathbf{b} \\ \mathbf{c} \end{pmatrix}_{\text{cubic}}$$

(i.e. lattice parameters of phase II are approximately equal to $a_{II} = \sqrt{3/2}a_{cub}$, $b_{II} = a_{cub}/\sqrt{2}$, $c_{II} = \sqrt{2}a_{cub}$, and $\beta_{II} \approx \cos^{-1}(-1/\sqrt{3}) = 126°$, but of course will differ slightly from these 'ideal' values because of spontaneous strains). At the wave vector **L** there are three rigid unit modes, two of which are doubly-degenerate by symmetry (Hammonds *et al.*, 1996). These rigid unit modes provide a natural displacive mechanism for the origin of the new monoclinic phase, and from the tables of Stokes and Hatch (1988) it appears that a rigid unit mode of either symmetry could condense to give the correct symmetry transformation.

In this paper we present results for the crystal structure of the high-pressure monoclinic phase-II from new high-pressure neutron powder diffraction data, and we show that the structure does indeed have space group $P2_1/c$. Before we present the experimental data, we show that the structure of phase-II can be predicted from energy minimization methods.

Independent prediction of the crystal structure of the high-pressure monoclinic phase

Empirical model calculations

Before performing the experiment, we used two independent model calculations to suggest trial structures for phase-II. Both calculations gave the same result, which suggests that the prediction of a trial structure is reasonably robust. Although we have noted that the space group of the monoclinic phase is likely to be $P2_1/c$ from group-theoretical reasoning, this information was not used in our model prediction. Instead, we started with the high-symmetry cubic structure, and projected this structure onto the monoclinic unit cell of Palmer and Finger (1994). We allowed this initial model to relax to an energy minimum using two methods and two interatomic potentials. First we gave some of the atoms small displacements, and allowed the structure to relax to an energy minimum by standard lattice energy minimization procedures, using the GULP program of Gale (1997) without any symmetry constraints, using the interatomic potentials of Sanders *et al.* (1984). After many cycles of minimization, this led to a structure from which the space group symmetry $P2_1/c$ could be inferred. From the final structure, an appropriate origin was calculated, and a set of atomic coordinates obtained.

The second approach was to use the initial model from the cubic structure in a molecular dynamics simulation, using the interatomic potentials of Tsuneyuki *et al.* (1988). For this work we used the program DLPOLY (Smith and Forester, 1996). The simulations were performed using samples containing 27 and 64 unit cells with periodic boundaries, using equations of motion appropriate to a constant-energy constant-volume ensemble. The simulations were run at initial temperatures of 400 K, and were then cooled in steps to 20 K. Analysis of the final atomic configurations showed that a single domain of a low-symmetry structure was obtained in each run, which was found to be equivalent to the structure obtained from the lattice energy minimization calculations except for a trivial shift in the origin. Trial structures for the crystal structure refinement were prepared merging the results from the two independent calculations.

Electronic structure calculations

We have checked the predictions of the empirical model calculations using two types of *ab initio* DFT electronic structure calculations. Both used pseudopotentials to represent the core electrons, but one used plane waves basis functions for the valence electrons (Payne *et al.*, 1992) and the other used localized atomic orbitals (Ordejón *et al.*, 1996; Artacho *et al.*, 1999). In both cases calculations were carried out using the local density (LDA) and generalized gradient (GGA) approximations. Convergence of the plane-wave

calculations was checked by using energy cut-offs up to 1000 eV, and the convergence of the atomic orbital calculations was checked by performing calculations using quadruple-ζ basis functions with polarization. Calculations with full relaxation of the structure were performed starting with the structures of both the tetragonal α-phase and the postulated monoclinic phase-II at pressures of 0 GPa and 2 GPa. Both structures were in a local energy minimum at both pressures, and the structures corresponded closely to the experimental structures (the experimental phase-II structure being that given in this letter). The calculations also suggested that the phase transition is first order, as observed experimentally. In the GGA both types of calculations gave the energy of the monoclinic phase of around 0.03 eV per monoclinic unit cell higher than the tetragonal cell. This energy difference was below 0.01 eV in the LDA plane wave calculations, and the LDA atomic orbital calculations gave the monoclinic structure having an energy lower by 0.12 eV. These differences are within the known errors associated with inaccuracies in the pseudopotentials, basis functions, and limitations of the LDA and GGA. It was not easy to compute the differences in volumes between the tetragonal and monoclinic structures with the same accuracy because small changes in volume have little effect on the energy but large effects on the volume differences. This is a result of the transition being driven by a RUM distortion, in which the structure can buckle with small cost in energy since there need be no accompanying distortions of the SiO_4 tetrahedra.

If we take the calculated energy difference of 0.03 eV, which translates to $\Delta E = 375$ J mol^{-1}, and take the experimental volume difference at the observed transition pressure of $\Delta V = -3 \times 10^{-7}$ m^3 mol^{-1} from Palmer and Finger (1994), we obtain an estimate for the transition pressure of $P_c = -\Delta E/\Delta V = 1.25$ GPa. This is in close agreement with the range of experimental transition pressures (Palmer and Finger, 1994; Onodera *et al.*, 1997), and gives us further confidence in the proposed crystal structure of the monoclinic phase. Further details of the electronic structure calculations will be published elsewhere.

Neutron diffraction experiments

The neutron diffraction experiments were performed on the High-Pressure (HiPr) facility of the PEARL beamline of the ISIS pulsed-neutron facility. High-pressures were obtained using a Paris-Edinburgh cell (Besson *et al.*, 1992; Nelmes *et al.*, 1993). A sample of powdered cristobalite, synthesized from silica glass, was mixed with Fluorinert® as the pressure-transmitting medium, and then loaded within a circular gasket made of from a titanium-zirconium alloy with composition that has zero coherent neutron scattering cross section. This was mounted between tungsten carbide anvils. Diffraction data were collected in time-of-flight mode from detector banks mounted at a scattering angle of 90°. Summing the spectra from the different detectors, normalization of the spectra with respect to the signal from a monitor on the incident beam and calibration measurements from a vanadium standard sample, and corrections to account for attenuation of the signal by the anvils and gasket were carried out using the method described by Wilson *et al.* (1995).

Initial sets of short measurements were made in increasing pressure up to 6 GPa, calibrating the pressure against the equation-of-state data of Downs and Palmer (1994) and Palmer and Finger (1994). We then obtained data obtained with longer counting times at four pressures above 1.6 GPa, and here we report results from one of these pressures, namely 3.5 GPa (data for other pressures will be presented in a later paper). Measurements at each of these pressures lasted about 18 hours. We note that because the geometry of our experiment and the pressure medium used differ from those employed by Downs and Palmer (1994) and Palmer and Finger (1994) there may be a small systematic offset in our pressure calibration. However, we do not anticipate that non-hydrostatic effects associated with the Fluorinert® pressure medium will significantly affect our results at 3.5 GPa.

Using the predicted crystal structure described above as a starting point, the structure was refined using the Rietveld method with the GSAS program (Von Dreele and Larson, 1986). All atomic coordinates and cell parameters, together with parameters in the functions to describe the background and peak shape, were refined. Contributions from Ni and WC were included as additional phases seen in the diffraction patterns. The final calculated diffraction pattern is compared with the experimental data in Fig. 1. The level of agreement is quite reasonable, except for difficulties in completely reproducing the most intense high-d peak (a common problem in

powder diffraction) and the failure to reproduce a broad feature in the diffraction pattern around d of 2.3 Å. This feature only occurs in the diffraction pattern for phase-II, and could be interpreted as a real feature of the diffraction pattern of phase-II. On the other hand, given that it is broader than the other Bragg peaks, it could arise from an artefact of the experiment. At the phase transition there is a sudden change in volume, which will cause a relaxation of the pressure apparatus. A small tail of the cadmium shielding that is used to mask the anvils from the neutron beam could have moved very slightly into the diffraction volume, giving a Bragg peak with a measured d-spacing that is not quite its actual value owing to the non-centring of the material in the beam. This is only a suggestion of one possibility, and it cannot be checked, but we are inclined to take such a suggestion seriously given the overall high level of agreement between the calculated and observed diffraction patterns.

In fact the model refined relatively easily, but led to some anomalously short and long Si–O bonds (given in Table 2 as described immediately below). This is a problem that can arise in the refinement of relatively complex structures from powder diffraction data, particularly given the

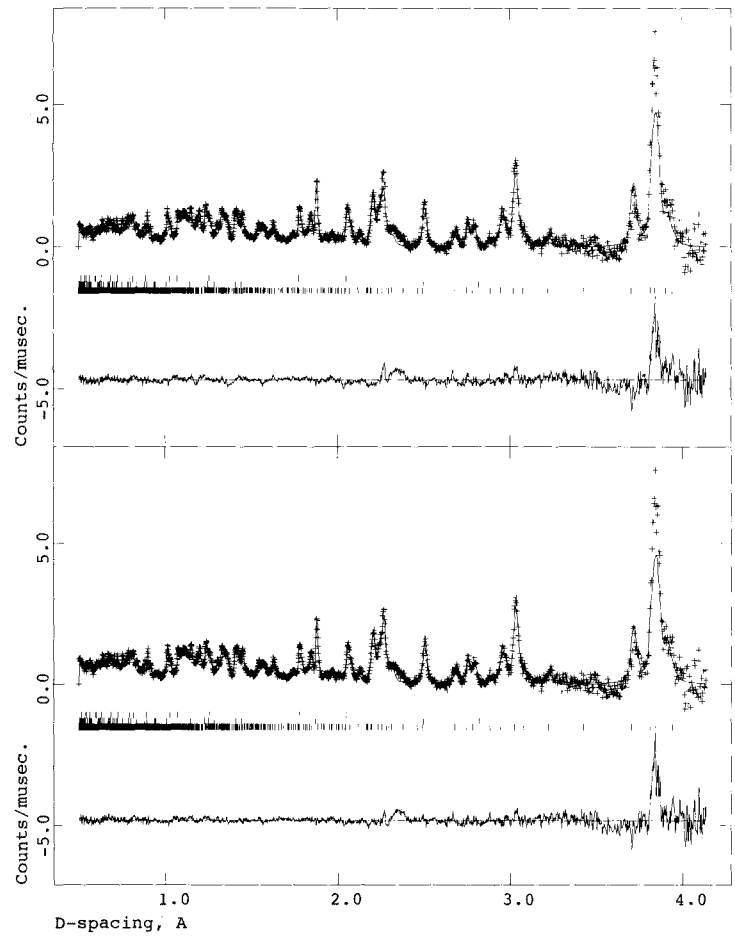

FIG. 1. Comparison of the fitted and experimental diffraction patterns for both unconstrained (top) and constrained (bottom) fits. The vertical tickmarks show the positions of the Bragg peaks, with the main series corresponding to the diffraction from phase-II of cristobalite, but with series from the unavoidable contributions from the WC anvils and the Ni binder.

TABLE 1. Lattice parameters and atomic fractional coordinates of phase-II cristobalite at 3.5 GPa obtained from unconstrained and constrained Rietveld refinements, with space group $P2_1/c$. The unweighted and weighted R-factors were 2.7% and 4.3% respectively for the unconstrained refinements, and 3.1% and 4.7% respectively for the constrained refinements.

	a (Å)	b (Å)	c (Å)	β (°)	Volume (Å^3)
Unconstrained	8.3780(11)	4.6018(6)	9.0568(13)	124.949(7)	286.21(4)
Constrained	8.3769(16)	4.6020(9)	9.0583(18)	124.939(11)	286.26(6)

	Unconstrained refinements				Constrained refinements			
	x	y	z	$100 \times U_{iso}$	x	y	z	$100 \times U_{iso}$
Si1	0.3726(11)	0.7339(16)	0.2187(9)	−0.18(9)	0.3725(3)	0.7310(8)	0.2145(4)	−0.03(13)
Si2	0.1340(10)	0.9779(13)	0.8529(10)	−0.18(9)	0.1207(4)	0.9699(9)	0.8403(4)	−0.03(13)
O1	0.1848(8)	0.8745(13)	0.0365(7)	0.28(6)	0.1859(5)	0.8645(11)	0.0351(4)	0.44(9)
O2	0.3056(9)	0.5954(13)	0.3331(7)	0.28(6)	0.2997(5)	0.5912(11)	0.3276(6)	0.44(9)
O3	0.5363(9)	0.9738(10)	0.3315(8)	0.28(6)	0.5296(7)	0.9791(11)	0.3297(4)	0.44(9)
O4	0.9304(9)	0.8052(12)	0.6908(7)	0.28(6)	0.927(5)	0.8089(9)	0.6839(4)	0.44(9)

complexity of the experimental apparatus that necessarily leads to lower resolution, lower intensity, and higher background as compared to other neutron powder diffraction instruments. Moreover, it is possible that problems due to non-hydrostatic pressure may give small distortions of the diffraction pattern that lead to difficulties in the refinements. The problem with bond lengths was overcome by using soft constraints on the Si–O and O–O bond lengths. The best mean bond lengths for the constraints were 1.595 Å and 2.605 Å for the Si–O and O–O distances, with tolerances of 0.02 Å and 0.04 Å respectively. The lattice parameters and atomic coordinates, without and with the constraints, are given in Table 1. The unit cell volume suggests a pressure of 3.5 GPa as calibrated against the data of Palmer and Finger (1994). The fitted diffraction pattern for the unconstrained refinement is shown in Fig. 1 (the pattern for the constrained refinement is not noticeably different). Bond lengths obtained from the refinements with and without the use of bond constraints are given in Table 2.

To test the sensitivity of the structure refinements on the diffraction pattern, we compared it with a model based only on the coordinates of the cubic phase projected onto the monoclinic unit cell. The calculated diffraction pattern from this model looked significantly different in many respects from the actual diffraction pattern, which reassured us that the data contains significant information beyond the change in the unit cell parameters!

TABLE 2. Bond lengths (in Å) within the SiO_4 tetrahedra, from the unconstrained and constrained refinements.

	Unconstrained	Constrained
Si1–O1	1.626(9)	1.598(3)
Si1–O2	1.569(9)	1.597(2)
Si1–O3	1.593(10)	1.597(2)
Si1–O3	1.619(9)	1.598(3)
Si2–O1	1.537(8)	1.594(1)
Si2–O2	1.583(8)	1.594(1)
Si2–O4	1.681(9)	1.598(3)
Si2–O4	1.572(8)	1.595(1)
O1–O2	2.603(8)	2.572(33)
O1–O2	2.563(9)	2.556(49)
O1–O3	2.646(8)	2.625(20)
O1–O3	2.663(8)	2.642(37)
O1–O4	2.608(8)	2.643(38)
O1–O4	2.612(8)	2.619(14)
O2–O3	2.608(7)	2.618(13)
O2–O3	2.560(8)	2.583(22)
O2–O4	2.620(8)	2.606(1)
O2–O4	2.666(8)	2.643(38)
O3–O3	2.610(5)	2.609(4)
O3–O3	2.610(5)	2.609(4)
O4–O4	2.524(5)	2.558(47)
O4–O4	2.524(5)	2.558(47)

Discussion

The crystal structure of the high-pressure monoclinic phase

The crystal structure of the high-pressure monoclinic phase-II (coordinates taken from the unconstrained refinement) is shown in two projections in Fig. 2. The first projection is down [0,1,0], which corresponds to the $[1,1,\bar{2}]$ direction of the cubic phase, and shows 6-membered rings of linked SiO_4 tetrahedra. In the cubic phase these rings are not perfect hexagons in the average structure. Rings of tetrahedra that form perfect hexagons are found in the $\{111\}$ layers of the cubic phase. One of these layers is seen in the second projection of the monoclinic phase shown in Fig. 2, which is along [1,0,3/2], and compared with the identical projection of the average cubic structure. This projection shows that there is considerable puckering of the rings due to the transformation to the monoclinic phase, which is accomplished by relatively large rotations of the tetrahedra.

The structure with the puckered hexagonal rings can be described using perfect SiO_4 tetrahedra. We used a simple model interatomic potential designed to produce perfect tetrahedra as an energy minimum (equivalent to a distance least-squares method). This calculation showed that our refined structure can easily be mapped onto a framework of perfect tetrahedra without the need for distortions of the tetrahedra.

The phase transition

We have remarked earlier that the general group-theoretical analysis of Stokes and Hatch (1988) gives the possibility of a phase transition from the

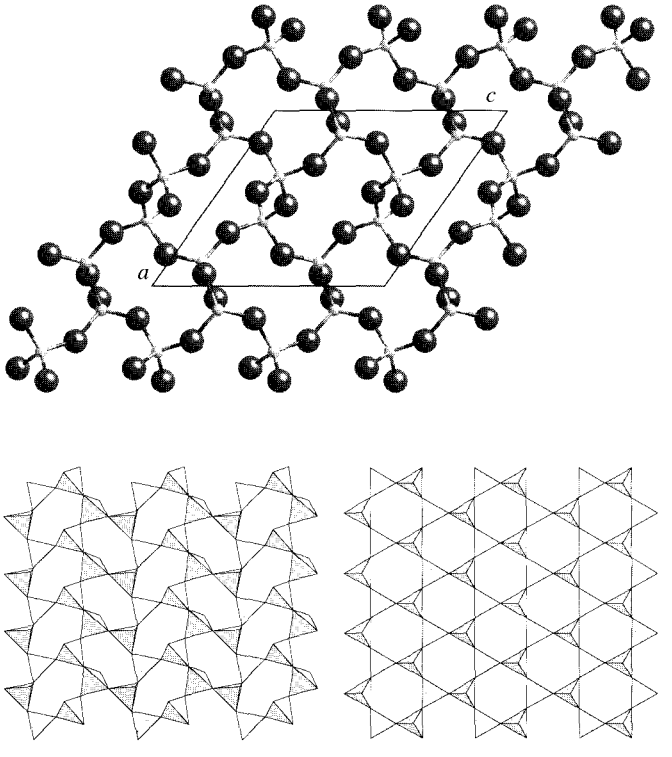

FIG. 2. Top: Crystal structure of the monoclinic phase-II of cristobalite viewed down [010], which corresponds to the $[1,1,\bar{2}]$ direction of the cubic phase. Bottom: Single layer of SiO_4 tetrahedra in the crystal structure of the monoclinic phase-II of cristobalite projected down [1,0,3/2], compared with a corresponding $\{111\}$ layer of the cubic phase in which the tetrahedra are arranged on average in perfect hexagons.

cubic β-phase to a monoclinic phase of space group $P2_1/c$ arising from a soft-mode with wave vector L = (½,½,½), and that this prediction is compatible with the predictions of the Rigid Unit Mode model (Hammonds *et al.*, 1996). The space-group symmetry $P2_1/c$ is not a subgroup of the space-group symmetry of the tetragonal phase, and therefore the phase transition does not involve a direct displacive instability of the tetragonal phase.

Our interpretation of the phase transitions in cristobalite is represented by a schematic energy surface in the phase space encompassed by the order parameters associated with the tetragonal and monoclinic distortions of the cubic phase, Fig. 3. We envisage that at low temperatures there are separate energy minima associated with the two structures (certainly our empirical and *ab initio* lattice energy calculations give these two minima). At low pressure the minimum associated with the tetragonal phase is the lowest energy structure. On increasing pressure the enthalpy of the monoclinic phase will be lowered relative to that of the tetragonal phase because of the lower volume of the monoclinic phase, until at a critical pressure the monoclinic phase will have the lower enthalpy and become the stable phase. At low temperatures there is always an energy maximum associated with the cubic phase, and a ridge of high energy always exists between the two minima. Thus the pressure-temperature phase diagram may have the form shown in Fig. 4.

We make this point in some detail because we believe that this type of behaviour may be more common for pressure-induced phase transitions than in temperature-induced phase transitions. In fact there are cases of temperature-induced phase transitions involving structures that are different distortions of a parent high-symmetry phase – tridymite (Pryde and Dove, 1998) and WO_3 (Salje *et al.*, 1997) are two examples. However, this type of behaviour is quite rare in the temperature case. Temperature has only a small effect on energies, and the primary driving force in temperature-induced phase transitions is entropy, with small differences in free energies between different phases. On the other hand, pressure always has the effect of changing bond lengths and volumes, which have a direct effect on energies, and therefore inverting of the ordering of energies of different phases is likely to be common.

The main result of this paper is the determination of the crystal structure of the monoclinic high-pressure phase-II of cristobalite using high-pressure neutron powder diffraction. This result shows the power of this experimental technique. It has also shown the power of the use of computational methods in the interpretation of experimental data. It is clear that had the diffraction data been interpreted in terms of a structure based on a distortion of the tetragonal

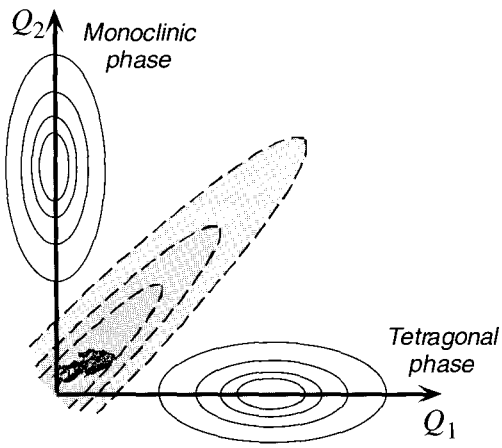

FIG. 3. Representative schematic energy surface on the phase space of the order parameters associated with the tetragonal (Q_1) and monoclinic (Q_2) distortions of the cubic phase, showing energy minima along the two axes and a maximum at the origin. The solid curves represent negative energies, and the dashed curves represent positive energies.

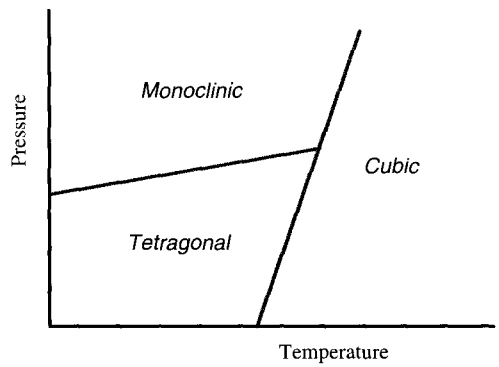

FIG. 4. Schematic representation of the predicted cristobalite pressure-temperature phase diagram.

α-phase, through a group-subgroup analysis, a successful result would not have been possible. The successful determination of the crystal structure was due to the ability of the computational models to predict the crystal structure of the new phase commensurate with its lattice parameters.

Acknowledgements

This work has been supported by EPSRC and NERC, the latter who also provided direct funding of the use of the ISIS facility. The molecular dynamics and electronic structure simulations were performed using the Hitachi SR2201 and Silicon Graphics Origin 2000 parallel computers of the Cambridge High-Performance Computing Facility. We are grateful to Emilio Artacho for help with the use of the SIESTA electronic structure code.

References

Artacho, E., Sánchez-Portal, D., Ordejón, P., García, A. and Soler, J.M. (1999) Linear-scaling ab-initio calculations for large and complex systems. *Physica Status Solidi (b)*, **215**, 809–7.

Besson, J.M., Nelmes, R.J., Hamel, G., Loveday, J.S., Weill, G. and Hull, S. (1992). Neutron powder diffraction above 10 GPa. *Physica B*, **180**, 907–10.

Downs, R.T. and Palmer, D.C. (1994) The pressure behaviour of α-cristobalite. *Amer. Mineral.*, **79**, 9–14.

Gale, J.D. (1997) Gulp: A computer program for the symmetry-adapted simulation of solids. *J. Chem. Soc. Faraday Trans.*, **93**, 629–37.

Hammonds, K.D., Dove, M.T., Giddy, A.P., Heine, V. and Winkler, B. (1996) Rigid unit phonon modes and structural phase transitions in framework silicates. *Amer. Mineral.*, **81**, 1057–79.

Nelmes, R.J., Loveday, J.S., Wilson, R.M., Besson, J.M., Klotz, S. Hamel, G and Hull, S. (1993) Structure studies at high pressure using neutron powder diffraction. *Trans. Amer. Crystallogr. Assoc.*, **29**, 19–27.

Onodera, A., Suito, K., Namba, J., Tanigucji, Y., Horikawa, T., Miyoshi, M., Shomomura, O. and Kikegawa, T. (1997) Synchrotron X-ray-diffraction study of α-cristobalite at high pressure and high temperature. *High Pressure Res.*, **15**, 307–19.

Ordejón, P., Artacho, E. and Soler, J.M. (1996) Self-consistent order-*N* density-functional calculations for very large systems. *Phys. Rev. B*, **15**, 10441–4.

Palmer, D.C., Hemley, R.J. and Prewitt, C.T. (1994) Raman spectroscoic study of high-pressure phase transitions in cristobalite. *Phys. Chem. Miner.*, **21**, 481–8.

Palmer, D.C. and Finger, L.W. (1994) Pressure-induced phase transition in cristobalite: an X-ray powder diffraction study to 4.4 GPa. *Amer. Mineral.*, **79**, 1–8.

Payne, M.C., Teter, M.P., Allan, D.C., Arias, T.A. and Joannopoulos, J.D. (1992) Iterative minimisation techniques for *ab initio* total-energy calculations: molecular dynamics and conjugate gradients. *Rev. Modern Phys.*, **64**, 1045–97.

Pryde A.K.A., and Dove M.T. (1998) On the sequence of phase transitions in tridymite. *Phys. Chem. Miner.*, **26**, 171–9.

Salje, E.K.H., Rehmann, S., Pobell, F., Morris, D., Knight, K.S., Herrmannsdorfer, T. and Dove, M.T. (1997) Crystal structure and paramagnetic behaviour of ε-WO_{3-x}. *J. Phys.: Cond. Matt.*, **9**, 6563–77.

Sanders, M.J., Leslie, M. and Catlow, C.R.A. (1984). Interatomic potentials for SiO_2. *J. Chem. Soc.: Chem. Comm.*, 1271–3.

Smith, W. and Forester, T.R. (1996). DL_POLY_2.0 – A general purpose parallel molecular dynamics simulation package. *J. Mol. Graphics*, **14**, 136–41.

Stokes, H.T. and Hatch, D.M. (1988) *Isotropy Subgroups of the 230 Crystallographic Space Groups*. World Scientific, Singapore.

Tsuneyuki, S., Tsukada, M., Aoki, H. and Matsui, Y. (1988). First principles interatomic potential of silica applied to molecular dynamics. *Phys. Rev. Lett.*, **61**, 869–72.

Von Dreele, R.B. and Larson, A.C. (1986) *Los Alamos National Laboratory Report*, LAUR 86-748.

Wilson, R.M., Loveday, J.S., Nelmes, R.J., Slotz, S. and Marshall, W.G. (1995). Attenuation corrections for the Paris–Edinburgh cell. *Nucl. Instr. Methods*, **354**, 145–8.

[*Manuscript received 8 February 2000: revised 19 April 2000*]